

ECRH AND ICRH IN THE TMX-U TANDEM MIRROR

B. W. Stallard, W. F. Cummins, A. W. Molvik,  
P. Poulsen, T. C. Simonen, S. Falabella,  
J. D. Barter, T. Christensen,  
G. Dimonte, and T. E. Romesser

This paper was prepared for submittal to the  
4th International Symposium on Heating in  
Toroidal Plasmas,  
Rome, Italy, March 21-28, 1984

March 15, 1984

Lawrence  
Livermore  
National  
Laboratory

This is a preprint of a paper intended for publication in a journal or proceedings. Since changes may be made before publication, this preprint is made available with the understanding that it will not be cited or reproduced without the permission of the author.

## DISCLAIMER

This document was prepared as an account of work sponsored by an agency of the United States Government. Neither the United States Government nor the University of California nor any of their employees, makes any warranty, express or implied, or assumes any legal liability or responsibility for the accuracy, completeness, or usefulness of any information, apparatus, product, or process disclosed, or represents that its use would not infringe privately owned rights. Reference herein to any specific commercial products, process, or service by trade name, trademark, manufacturer, or otherwise, does not necessarily constitute or imply its endorsement recommendation, or favoring of the United States Government or the University of California. The views and opinions of authors expressed herein do not necessarily state or reflect those of the United States Government or the University of California, and shall not be used for advertising or product endorsement purposes.

## ECRH AND ICRH IN THE TMX-U TANDEM MIRROR

B. W. Stallard, W. F. Cummins, A. W. Molvik, P. Poulsen, and T. C. Simonen  
Lawrence Livermore National Laboratory, University of California  
P. O. Box 5511, Livermore, CA 94550

S. Falabella  
University of California, Davis, CA 95617

J. D. Barter, T. Christensen, G. Dimonte, and T. E. Romesser  
TRW Corporation, Redondo Beach, CA 90278

### ABSTRACT

In the Tandem Mirror Experiment Upgrade (TMX-U), the formation of a thermal barrier and the potential plugging of ion end loss were achieved at central-cell densities up to  $2 \times 10^{12} \text{ cm}^{-3}$ . The presence of a thermal barrier was confirmed by direct measurement, and ion axial-confinement times in the range 50 to 100 ms were measured. The ECRH in the end cells (a) initiates plasma startup, (b) generates hot, mirror-confined electrons to form thermal barriers, and (c) creates the plugging potential for central-cell ions. The ECRH system consists of four 200 kW, 28 GHz gyrotrons each feeding power to a separate heating location (two in each end plug). Fundamental heating is used at the potential plug, and second harmonic is used in the thermal barrier. Hot-electron plasmas are produced at total end-cell antenna power levels up to 300 kW. Strong single-pass absorption and net hot-electron heating efficiencies exceeding 40% are observed. Hot-electron parameters achieved are:  $n_{eh}/n_{et}$  up to 0.8, volume-average beta  $\langle \beta \rangle \approx 0.15$ , and  $T_x$  (x-ray "tail" above 40 keV) in the range 75 to 200 keV.

We employ ICRH to heat central-cell ions. For ion heating in the frequency range 1.7 to 4 MHz, the ICRH antenna launches the slow wave for fundamental absorption at power levels up to 100 kW. At a central density  $n_c = 2 \times 10^{12} \text{ cm}^{-3}$  and frequency  $\omega/\omega_{ci} = 0.85$  at the antenna, 100 kW antenna power produced a mean perpendicular ion temperature  $T_{ic\perp} = 1.5 \text{ keV}$  with overall efficiency of 40%.

### Introduction

The ECRH is employed for plasma heating in tandem mirror devices with thermal barriers to improve plasma confinement /1/. The ICRH is useful for heating central-cell ions and is important particularly during startup for increasing the ion temperature at low density when neutral beam heating is inefficient.

We compare a tandem mirror with thermal barriers to a standard tandem in Fig. 1 /2/. In the latter device, reduction of central-cell end losses by potential plugging is accomplished by increasing the end-cell density ( $n_p$ ) above the central-cell density ( $n_c$ ). The plugging potential is given by a Boltzmann relation,  $\phi_c = T_e \ln n_p/n_c$ , where  $T_e$  is the electron temperature. An improvement in confinement by a factor 10 for this mode of operation over unplugged flow confinement was demonstrated in the TMX device /3/.

With the addition of thermal barriers and localized plug electron heating, the confining potential can be created with plug density lower than central-cell density. The lower plug density relaxes technology constraints and improves the economics for a tandem mirror reactor.

The thermal barrier is created by a mirror-trapped population of hot electrons heated by ECRH. Replacement of non-trapped electrons (passing electrons) by mirror-trapped electrons causes the potential at the well bottom to decrease because trapped electrons are well confined. The depth of the potential dip is determined by the fraction of electrons that are mirror-trapped in the barrier ( $\sim 0.8$  for TMX-U). The thermal barrier (potential dip) isolates central-cell electrons from electrons beyond the barrier. If these electrons are heated by ECRH, the potential is driven up by the increased loss rate of electrons until the ion- and electron-loss rates are made equal. The electron density beyond the barrier is set by the density of energetic sloshing ions created by neutral beam injection. The energetic ions are required for MHD stability and, in addition, their sloshing character improves ion microstability.

Maintenance of the thermal barrier against collisional filling by ions that circulate between the central cell and end plug is achieved by charge-exchange "pumping" on the injected sloshing-ion neutral beams. The maximum pumping rate determines the relation between central-cell ion density and temperature (filling rate  $\propto n^2/T_{ic}^{3/2}$ ). Central-cell neutral beam heating, as well as ICRH in the central cell, serves the important function of increasing the central-cell ion temperature as density is raised to decrease barrier filling by reducing ion collisionality.

The TMX-U experiment was designed to test the thermal barrier principle. A schematic of the experiment is shown in Fig. 2. Four 28 GHz, 200 kW pulsed gyrotrons are used for electron heating; fundamental heating is used in the plug ( $B = 10$  kG at the high potential region) and  $2\omega_{ce}$  harmonic heating in the thermal barrier ( $B = 5$  kG). For ICRH experiments reported in this paper a maximum 100 kW transmitter power with frequency in the range 1.7 to 4 MHz has been used.

There are 24 neutral beam modules on the experiment with nominal operating parameters of 17 kV and 50 A per module for deuterium operation. In each end cell, six beams are injected at  $47^\circ$  to the magnetic axis to generate sloshing ions. Three beams are available in each end to inject into the loss cone for auxiliary charge-exchange pumping of the thermal barrier. The remaining six beams fuel and heat the central-cell plasma.

In this paper we summarize our initial experiments on using ECRH for startup of the thermal barrier. Formation of the thermal barrier and potential plugging of ion end losses was achieved at central-cell densities up to  $2 \times 10^{12} \text{ cm}^{-3}$ . This density is dictated by the requirements on ECRH and ICRH power and by the maximum available neutral-beam pumping rates against thermal barrier filling. The ECRH power required for trapping and heating hot electrons, in competition against collisional losses, scales as  $P_{\text{ECRH}} \propto n_e^2/T_e^{1/2}$ . During startup when temperatures are initially low, the density must also be low for efficient heating. As rf power coupled to the plasma was increased, we were able to raise plasma density in both the central cell and the end cells. Future experiments will continue to increase the central-cell density to 1 to  $2 \times 10^{13} \text{ cm}^{-3}$ .

#### ECRH and ICRH Heating Systems

Two different ECRH transmission and antenna systems were used on the experiment. The first system used an 8-arm phase-velocity coupler designed to couple  $\text{TE}_{02}$  gyrotron power into WR42 single-mode waveguide [4]. Each waveguide ( $\sim 3 \text{ m}$  in length) was connected to a highly directional microwave horn for illumination of the plasma. Figure 3 shows a schematic of each system used for plug and thermal barrier heating in one end cell. At both locations, the wave was launched with extraordinary mode polarization.

For fundamental heating this required high-field launching of the wave for accessibility to the resonant magnetic surface. Vacuum barrier windows were located near the ends of the waveguides. The plasma is highly elliptical in cross section at fundamental resonance because of the quadrupole fields (min-B) needed for MHU stability of the plasma.

The 8-arm coupler system delivered  $\sim 50\%$  of the gyrotron tube power to the antennas ( $\sim 70\%$  waveguide transmission and  $\sim 70$  to  $75\%$  coupler efficiency). The typical operating antenna-power level per system was 50 to 60 kW, limited by component arcing and window failure.

To reduce system losses and to allow operation at full gyrotron power, we replaced each 8-arm coupler system with a large waveguide transmission system, mode converter, and polarizing antenna. The thermal barrier system ( $\omega \approx 2 \omega_{ce}$ ) is sketched in Fig. 4. Gyrotron power is converted from the  $TE_{02}$  to the  $TE_{01}$  mode in a 2-1/2-in. waveguide using an  $m = 0$  rippled-wall mode converter /5/. The waveguide output illuminates a focusing twist reflector, shown in Fig. 5, which converts the  $TE_{01}$  mode to linear polarization and focuses the power onto the plasma /6/. The percentage of beam power from the plate in the extraordinary mode is about 95%. Routine operation up to 200 kW of gyrotron output was achieved with this system, with 85 to 90% of tube power in the desired polarization.

For plug heating ( $\omega \approx \omega_{ce}$ ), a Vlasov-type polarizing reflector /7/ is used in place of the twist reflector. This system includes a down taper to 1-3/8 in. waveguide, corrugated waveguide  $90^\circ$  bends for the  $TE_{02}$  mode /8/ and a rippled-wall mode converter ( $TE_{02} \rightarrow TE_{01}$ ), followed by the Vlasov reflector. We have operated the system to over 100 kW of antenna power.

For the ICRH experimental results reported in this paper, the antenna shown in Fig. 6 was used. The antenna winding consists of two opposing  $170^\circ$  segments, each consisting of 3 turns, behind a double-layer Faraday shield. This antenna was used at 100-kW-power level for the frequency range 1.7 to 4 MHz. Ion heating in the central cell occurs using slow wave heating at the fundamental for deuterium.

#### Thermal Barrier Formation and Plugging of Ion End Loss

Formation of a thermal barrier and plugging of ion end loss requires (1) a hot, mirror-trapped electron population, (2) a sloshing ion-population, and (3) ECRH at the outer peak of the sloshing ion population. An experimental shot that demonstrates plugging of ion end loss and that shows the time sequence of the experiment is shown in Fig. 7. The experiment is initiated by ECRH breakdown of a gas source in the central cell. Hot-electron diamagnetism rapidly increases in the end plug. At 25 ms, the sloshing neutral-beam sources are turned on. After several ms the ion end losses start to decrease, as measured by a Faraday cup array. The time required for strong reduction of end losses equals the buildup time for the sloshing ions. Plugging persists for 20 ms until turnoff of the ECRH power. During plugging, the confinement time for ion end loss is  $\tau_{ijl} \sim 50$  to 100 ms. Ion end losses then rapidly increase on a time scale  $\sim 1$  ms. The time scale for loss of plugging is consistent with estimated electron-electron scattering times.

The requirement that a large percentage of electrons be mirror-trapped for plugging to occur is demonstrated in Fig. 8. The hot-electron density, calculated from a measurement of hot-electron diamagnetism and a measurement of temperature by a calibrated radiometer, is plotted as a function of total density in the thermal barrier for shots with and without plugging. With one

exception, plugging occurs only for shots with  $n_h/n_{tot} > 0.8$ , in good agreement with the thermal barrier plugging model.

In Fig. 9 we show the results of direct measurements on a single shot of the potential profile during plugging [9]. These confirm the existence of a thermal barrier and a potential peak. The measurements were performed by operating the experiment single-ended with plugging in one end cell. For the measurement, we used three gridded end-loss analyzers, whose ion-repelling grid is swept in voltage to measure ion energy distributions, and a 5-keV neutral beam injected into the loss cone of the end cell.

On the end without plugging, Analyzer 1 measured the energy of escaping ions from the central cell. These ions escape with a minimum energy equal to the central-cell potential,  $\phi_e = 1$  kV. Analyzer 2 measures the energy of ions born by charge exchange on a 5-keV neutral beam injected at the plugging end. Charge exchange on this beam extends from just beyond the thermal barrier minimum to the central cell. These ions have energy  $\phi_e - \phi_b \leq E_i - 5 \leq \phi_e$ . Thus, the depth of the barrier, as well as a second independent measurement of  $\phi_e$ , is obtained. The measured depth of the barrier was  $\phi_e - \phi_b = 500$  V. Finally, Analyzer 3 measures the energy of ions escaping out the plugging end. For this measurement, the peak potential  $\phi_p$  exceeded 2.4 kV, the limiting voltage available on the ion-repeller grid. The measured potentials, with error bounds of  $\pm 100$  V, agree with the predictions of the thermal barrier model.

TABLE I summarizes the plasma parameters for which end plugging was observed. Other measurements showed plugging when the central-cell density exceeded the plug density by a factor 1.5, a result which further supports the thermal barrier model.

TABLE 1. Plasma parameters for end-loss plugging.

Region	Parameter	Range of values
Central cell	Density, $n_c$	Up to $2 \times 10^{12} \text{ cm}^{-3}$
	Electron temperature, $T_{ec}$	30 - 200 eV
	Ion temperature, $T_{ic}$	50 - 200 eV
	Plasma potential, $\phi_e$	Up to 1400 V
	Confining potential, $\phi_c$	> 1400 V
Potential plug	Density, $n_p$	$1 - 2 \times 10^{12} \text{ cm}^{-3}$
	Potential, $\phi_p$	> 2400 V
Thermal barrier	Hot electron fraction, $n_{eh}/n$	$\sim 0.3$
	Hot electron density, $n_{eh}$	$> 1.5 \times 10^{12} \text{ cm}^{-3} *$
	Temperature, $T_{eh}$	30 - 200 keV **
	Barrier depth, $\phi_e - \phi_b$	Up to 600 V

\* Lower limit estimated from X-ray spectra above  $\sim 40$  keV.

\*\* Hot electron "tail" temperature from x-ray spectra above 40 keV.

#### Hot-Electron Production by ECRH

The generation of the hot-electron component in the thermal barrier was studied theoretically and experimentally for a range of plasma parameters. Fokker-Planck and Monte-Carlo computer calculations give insight into the heating processes /10/. Fundamental ECRH, in addition to creating the potential peak, is believed to be important for supplying the "feed" population for the thermal barrier electrons. Cold passing electrons from the central cell are trapped by strong rf diffusion in the end cells. In TMX-U, with power injected only at the fundamental, electrons are rapidly heated to average energies in the range of 5 to 10 keV, as deduced from measurements of diamagnetism and density. These electrons in turn are further heated to much higher energy by harmonic heating near the magnetic minimum.

The primary diagnostics for hot electrons are diamagnetic loops, x-ray bremsstrahlung, radiometers looking both perpendicular and near parallel to the magnetic field to measure plasma emission, and interferometers to measure plasma line density.

The scaling of hot-electron beta with ECRH power is plotted in Fig. 10. The volume-averaged beta  $\langle\beta\rangle$  increases in proportion to antenna input energy over more than an order of magnitude. The time variation of diamagnetism for the largest hot-electron beta observed in TMX-U is also shown in the figure. This shot achieved 15% average beta, even though equilibrium was not yet achieved with 50 ms duration of ECRH power. For a 140-litre hot-electron volume, the net conversion efficiency from rf power to stored energy was 0.42 during the initial use. The final ratio of stored energy to input energy was 0.30. More typically it is about 0.15.

To determine the axial extent of the hot electrons, we used an array of three diamagnetic loops, spaced along the magnetic axis. These measurements fit a Gaussian of 64 cm half-width scale length. For the radial dimension, a scraper probe was moved radially for a series of shots. A parabolic radius of 20 cm is inferred from the diamagnetic loops. A simultaneous decrease in perpendicular plasma emission is in agreement with the loop data. The resulting density-weighted, hot-electron volume is  $V_h \approx (\sqrt{\pi} 64) \pi(20)^2 \approx 140$  litre.

From Fokker-Planck calculations, we found buildup of hot electrons by rf trapping of passing electrons to be dependent on central-cell density /10/. If the density is too low, trapping is source limited. If density is too high, the trapping efficiency decreases because of collisional losses. These effects are shown in Fig. 11 with ECRH power as a parameter. The heating rate is measured from the rate of rise of diamagnetism at constant

density. For the 8-arm coupler system and 50-kw antenna power at both resonances, maximum efficiency occurs for a central-cell density  $n_c \lesssim 1 \times 10^{11} \text{ cm}^{-3}$ . At four-times higher power in the thermal barrier, using the large waveguide system, the peak efficiency occurs at density  $n_c \lesssim 1 \times 10^{12} \text{ cm}^{-3}$ . At the higher power level, central-cell electron temperatures measured by Thompson scattering were in the range 40 to 100 eV. As electron temperature increases with improved plasma confinement, the density for peak heating efficiency is also expected to increase.

The theoretical single-pass fractional absorption of ECRH power in the thermal barrier is near unity for TMX-U hot-electron densities. This is confirmed by measurement of beam transmission in the thermal barrier using an array of waveguide probes located on the plasma side opposite to the twist reflector antenna. These waveguides view transmission through chords of the plasma.

We show in Fig. 12 diamagnetism, thermal barrier ECRH transmission through the plasma center ( $y = 0$ ), plasma line density, and perpendicular plasma emission for a shot that reaches a maximum beta,  $\langle \beta \rangle \approx 0.09$ . Before gas breakdown, the unattenuated receiver ECRH power is 200 W. Coincident with the rise of diamagnetism, there is an abrupt decrease of transmission. For the remainder of the pulse, transmission varies from about zero to 40%. Fluctuation of transmission correlates with variation in the diamagnetism rate of rise and the line density. Plasma emission initially rises rapidly and then increases more slowly after 20 ms. The non-thermal burst emissions seen in the 35-GHz radiometer signal are evidence for hot-electron microinstability. However, no large losses or limits on heating were observed because of these instabilities. Following

turnoff of the thermal barrier ECRH at 55 ms, the diamagnetism decays even though the fundamental power is left on until 65 ms.

The ECRH transmission through plasma chords is generally greater than through the diameter, which is consistent with peaking of hot-electron density on axis. Measurements of x-ray bremsstrahlung spectra at energies greater than  $\sim 40$  keV reveal a hot-electron "tail" temperature reaching 176 keV at the end of the pulse. The density of the tail corresponds to  $\sim 7 \times 10^{11} \text{ cm}^{-3}$ , an estimated 30 to 40% of total density. At electron temperature above 50 to 75 keV, the interferometer is not an accurate measurement of density because of relativistic corrections in the dielectric constant [11]. Thus, the interferometer data decays more rapidly than the diamagnetism because of loss of lower energy electrons.

X-ray temperatures and densities measured for other shots vary over the range 75 to 200 keV and up to  $1.5 \times 10^{12} \text{ cm}^{-3}$ , respectively. The x-ray spectra below 40 keV was not measured for this data. We expect a non-Maxwellian hot-electron distribution from the Fokker-Planck and Monte Carlo models. Thus, we believe that the hot-electron density estimated from present x-ray data is a lower limit on total mirror-trapped density.

We calculated absorption in the thermal barrier, using a relativistic ray-tracing code which includes harmonics  $l \geq 2$  [12]. Preliminary calculations obtained by using an approximate model for the TMX-U magnetic field are plotted in Fig. 13. These calculations were carried out for a constant density  $n = 1 \times 10^{12} \text{ cm}^{-3}$  and for temperatures from 5 to 100 keV. As the temperature was increased, the effect of plasma beta was simulated by reducing the magnetic field uniformly by a factor  $\sqrt{1 - \langle \beta \rangle}$ . The microwave beam is launched near the magnetic minimum ( $z = 0$ ) through the thin side of the plasma fan. The waveguide array that views the transmitted power samples rays for  $N_{\parallel} \ll 1$ .

From the calculations we see that refraction is negligible and that absorption is strong, even for  $T_e = 5$  keV. This is due to the large magnetic scale length  $L_B \approx 500$  cm. As temperature increases, absorption first decreases and then increases. At 100 keV, absorption is strong and insensitive to spatial location. While these model calculations are only a rough approximation to the TMX-U experiment, they are consistent with experimental measurements and predict absorption of the same order of magnitude.

#### Central-Cell Heating by ICRH

Experiments to heat central-cell ions in the low density range of  $10^{12}$  cm<sup>-3</sup> were carried out using the antenna shown in Fig. 6 /13/. One advantage of ICRH is the efficient ion heating at low density, which aids thermal barrier startup when neutral beam trapping efficiencies are low.

In TMX-U we couple up to 100 kW of transmitter power into the antenna at densities up to  $2 \times 10^{12}$  cm<sup>-3</sup>. A data shot at 100 kW of antenna power and central-cell density of  $2 \times 10^{12}$  cm<sup>-3</sup> is shown in Fig. 14. The transmitter frequency was 2.48 MHz, corresponding to  $\omega/\omega_{ci} = 0.85$  at the antenna and 1.06 at the central-cell midplane. During the rf pulse, the mean perpendicular ion temperature, as measured by diamagnetism, increased to  $T_{\perp ci} = 1.5$  keV. Of the total 100 kW antenna power, 72 kW was radiated and 40 kW appeared as ion diamagnetism, an overall ion-heating efficiency of 40%. Ion lifetimes were in the range 2 to 4 ms, which we believe is limited by charge exchange and electron drag.

During the rf pulse we also measure an approximate increase by a factor of 2 in parallel ion temperature, from 75 to 150 eV, for ions lost out the ends. Since ions are heated by ICRH near the magnetic field minimum, their

anisotropy is large,  $T_{i\perp} \gg T_{i\parallel}$ . During the average lifetime of 2 to 4 ms, there is insufficient collisional angular scattering to reach a distribution that fills out to the mirrors, even though an off-midplane diamagnetic loop shows evidence of angular broadening. We believe this accounts for the smaller increase of parallel ion energy for escaping ions compared to the increase in perpendicular energy.

### Summary

Our initial experiments to improve tandem mirror confinement with thermal barriers confirm the essential features of the thermal barrier model. We have measured both the dip in potential at the barrier and the potential peak in the end cell that exceeds the central-cell potential. Hot mirror-confined electrons in the thermal barrier, a sloshing ion population in the end cell, and electron heating at the outer peak of the sloshing ions are required for plugging of end losses. Axial ion confinement times  $\tau_{i\parallel}$  in the range 50 to 100 ms were measured. Depending on operating conditions, non-ambipolar radial transport confinement times ranging from 5 to 100 ms were observed. Because this radial transport appears most strongly driven by fundamental ECRH, we are exploring more uniform and azimuthally symmetric heating schemes.

Generation of hot electrons by using ECRH and heating central-cell ions with ICRH was achieved with efficiencies up to 40%. As the rf power was increased, the central-cell and end-cell density for end-loss plugging was also increased. Figure 15 summarizes operation at higher central-cell density with increases in ECRH and ICRH power.

We expect further increases in density by (a) improvement in plasma core heating by reorienting neutral beams in the central cell, (b)

improvement in central-cell vacuum to reduce losses against charge exchange, and (c) addition of a second ICRH antenna system, a slotted antenna /13/ of improved efficiency, to the central cell to increase rf heating power.

#### Acknowledgements

The results reported in this paper are due to the efforts of many persons in the TMX-U experimental group. The author would like to particularly acknowledge D. P. Grubb for the measurements of plasma potential; R. A. James and C. J. Lasnier for radiometry measurements; J. F. Clauser, B. M. Failor, and E. H. Silver for x-ray measurements; and W. E. Nexsen for the diamagnetic-loop measurements.

This work was performed under the auspices of the U.S. Department of Energy by the Lawrence Livermore National Laboratory under contract number W-7405-ENG-48.

REFERENCES

- /1/ BALDWIN, D. E. and LOGAN, B. G., Phys. Rev. Lett., 43 (1979) 1318;  
COHEN, R. H., et al., Nucl. Fusion, 20 (1980) 1421; COHEN, R. H., Phys. Fluids, 26 (1983) 2774.
- /2/ DIMOV, G. I., et al., Sov. J. Plasma Phys., 2 (1976) 326; also FOWLER, T. K., and LOGAN, B. G., Comments Plasma Phys. Controlled Fusion, 2 (1977) 167.
- /3/ CORRELL, D. L., et al., Nucl. Fusion, 22 (1982) 223.
- /4/ Coupler designed by C. P. MOELLER, General Atomic Co., San Diego, CA.
- /5/ KOVALEV, N. F., et al., Izv. Vyssh. Vchebn. Zaved., Radiofiz. [Sov. Radiophys.] 11 (1968) 783; also THUMM, M., Institut für Plasmaforschung der Universität Stuttgart, F.R.G., private consultation.
- /6/ COFFIELD, F. E., et al., Proc. 10th IEEE Symp. on Engr. Problems of Fusion Res., Philadelphia, PA, Dec. 1983, in press.
- /7/ VLASOV, S. N. and ORLOVA, I. M., Izv. Vyssh. Vchebn. Zaved., Radiofiz. [Sov. Radiophys.] 17 (1974) 148.
- /8/ DOANE, J. L., Princeton Plasma Physics Laboratory, Princeton, N.J., private consultation.
- /9/ GRUBB, D. P., et al., Submitted to Phys. Rev. Lett.
- /10/ STALLARD, B. W., et al., Nucl. Fusion, 23 (1983) 213; also MATSUDA, Y., and ROGNLIEN, T., Phys. Fluids, 26 (1983) 2778.
- /11/ BATCHELOR, D. B., et al., Bull. Am. Phys. Soc. 27 (1982) 1078.
- /12/ Computer Absorption Code provided by BATCHELOR, D. B. and GOLDFINGER, R. C., Oak Ridge National Laboratory, Oak Ridge, Tenn.
- /13/ MOLVIK, A. W., et al., paper C28 this conference.

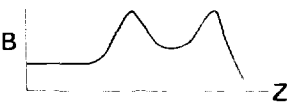
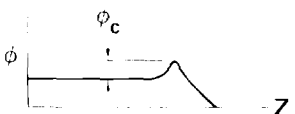
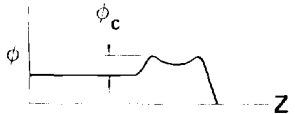
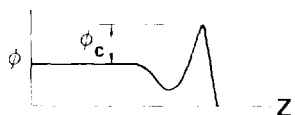
	Input power	Potential confinement	End cell ion microstability (source of low energy ions)
<p>Original tandem mode</p> 	90° beams	$\phi_c = T_e \ln \left( \frac{n_p}{n_c} \right)$	Center cell ion losses
<p>Sloshing ion mode</p> 	47° beams	$\phi_c = T_e \ln \left( \frac{n_p}{n_c} \right)$	Potential trapped ions and central cell ion losses
<p>Thermal barrier mode</p> 	ECRH 47° beams pump beams	Strong ECRH $\phi_c \approx T_{ec} \left[ \left( \frac{n_p}{n_b} \right)^{2/3} - \ln \left( \frac{n_c}{n_b} \right) \right]$	Potential trapped ions and passing center cell ions

Fig. 1. Tandem mirror operating modes.

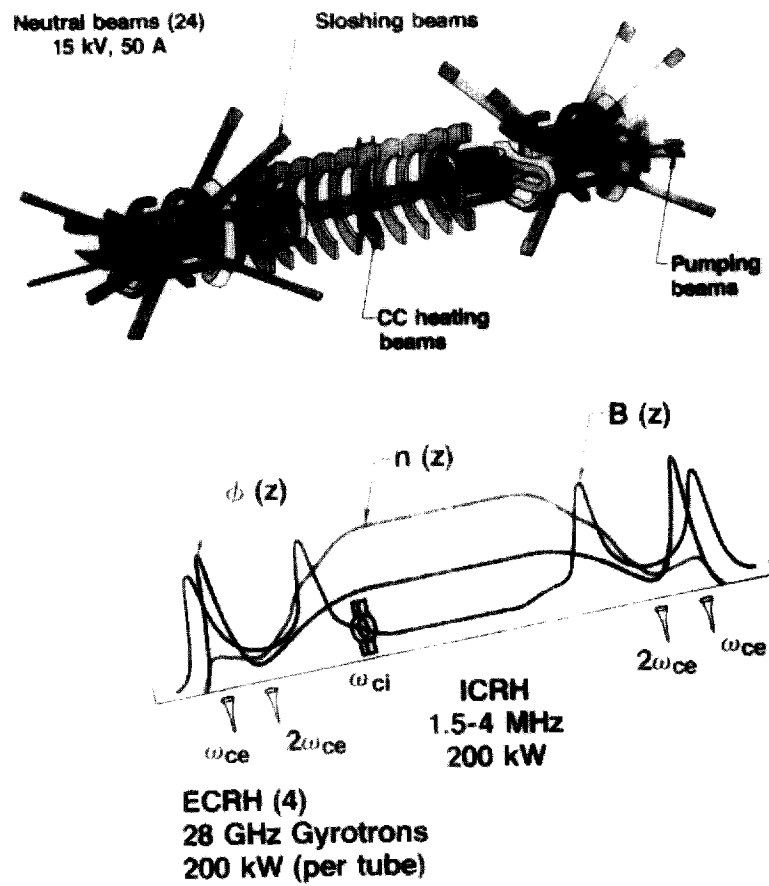


Fig. 2. M2F axial field fusion reactor. Location of heating and neutral beam injection. The diagram shows the beam locations.

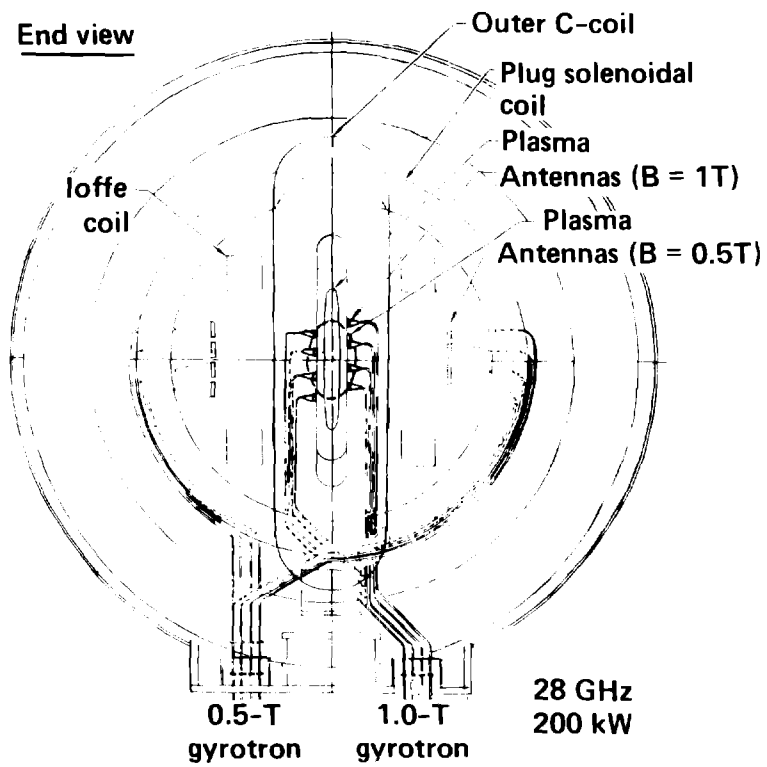


Fig. 3. Microwave antennas in end cell of TMX-U powered by 8-arm coupler.  
The plasma cross-sections are shown at each heating location.

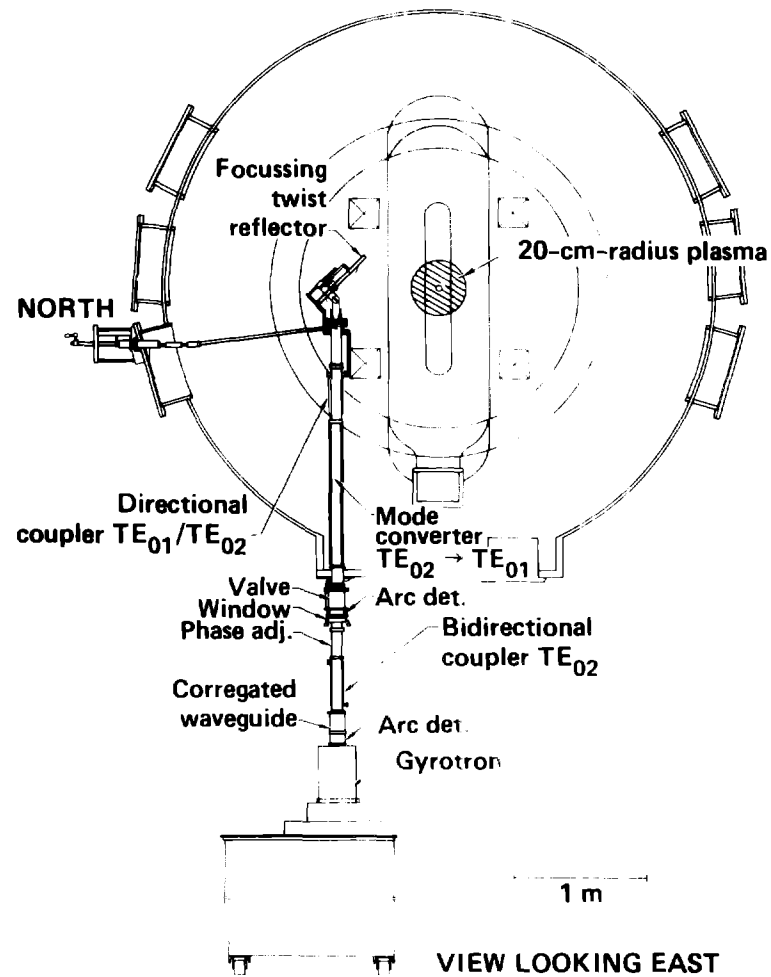


Fig. 4. Large waveguide system in TMX-U employing focussing twist reflector for thermal barrier heating.

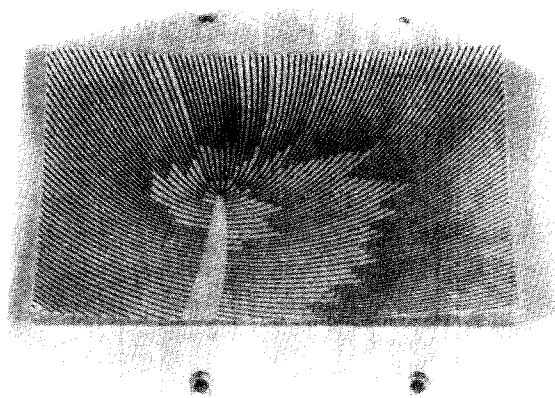


Fig. 5. Photograph of focusing telescope for the grooved section.  
dimensions are 77 cm x 34 cm.

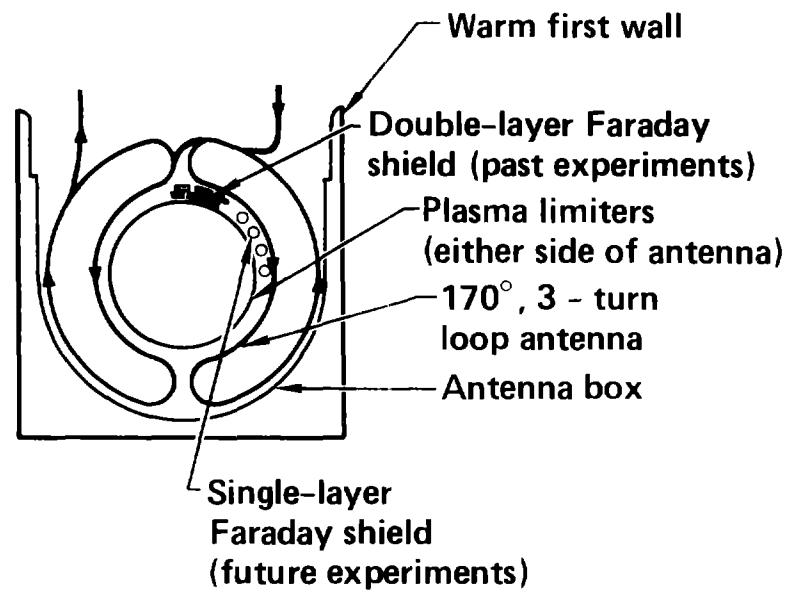


Fig. 6. ICRH antenna for TMX-U central cell heating. Two 170<sup>0</sup> segments are driven in series.

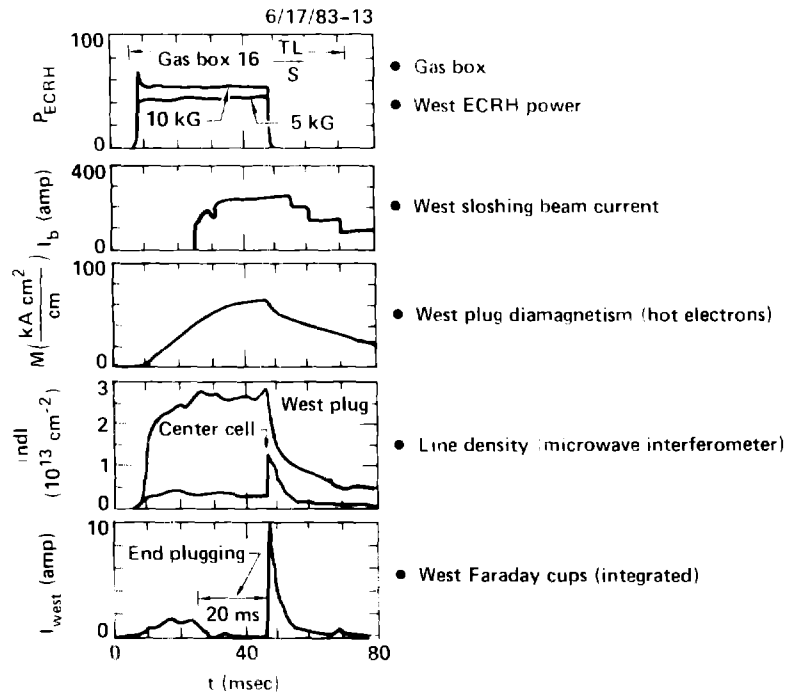


Fig. 7. Ion end-loss plugging in TMX-U for thermal barrier mode of operation.

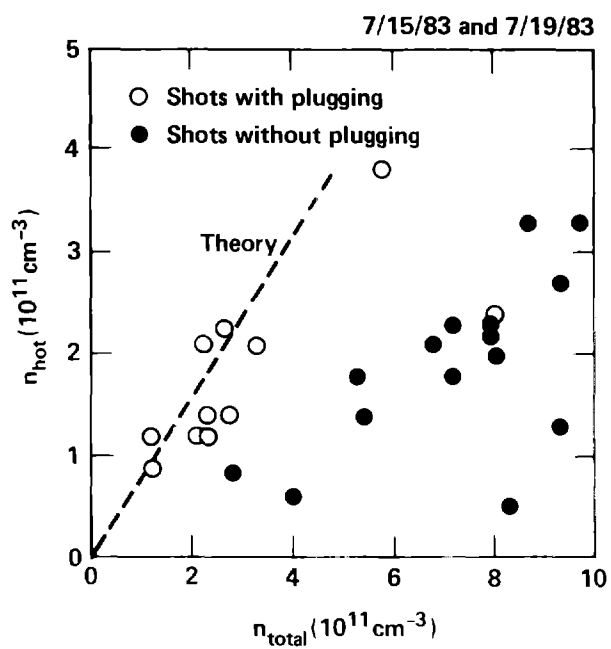


Fig. 8. Correlation of hot-electron density against total density in the thermal barrier for shots with and without plugging in TMX-U.

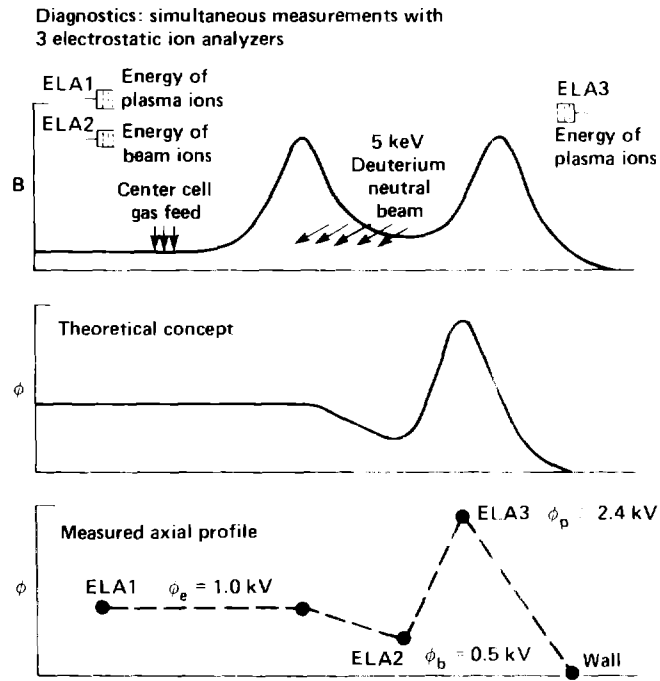


Fig. 9. Potential measurements in TMX-U confirming existence of thermal barrier and potential peak. The measured depth of the thermal barrier is  $\phi_e - \phi_b \approx 500$  V.

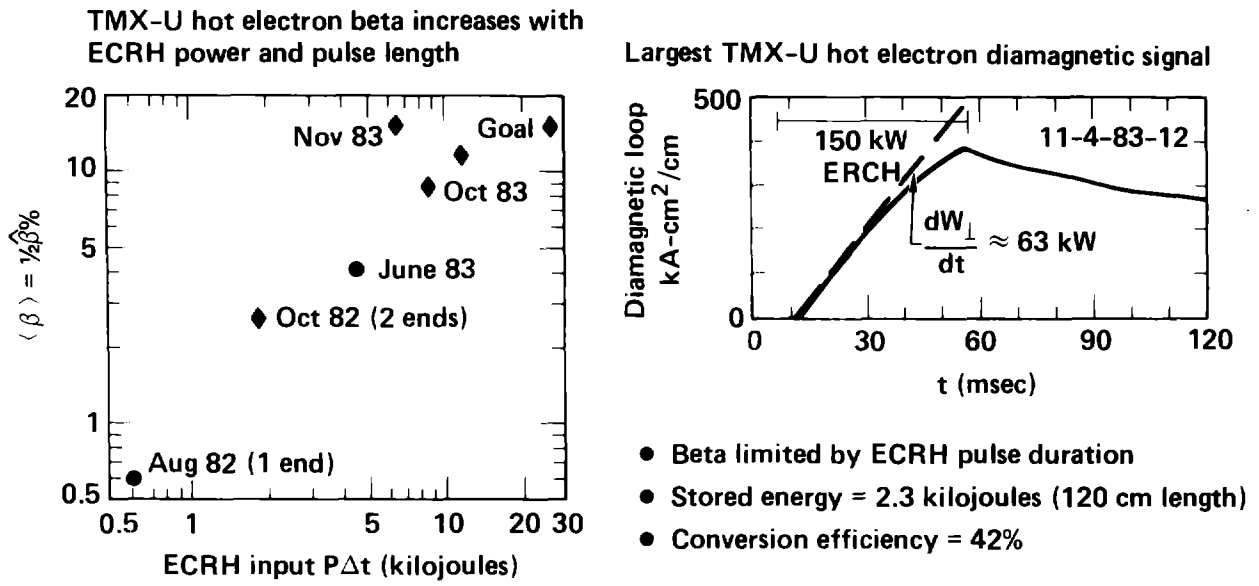


Fig. 10. Scaling of hot-electron beta with ECRH energy input. A shot with 15% average beta is shown, with 42% initial heating-rate efficiency.

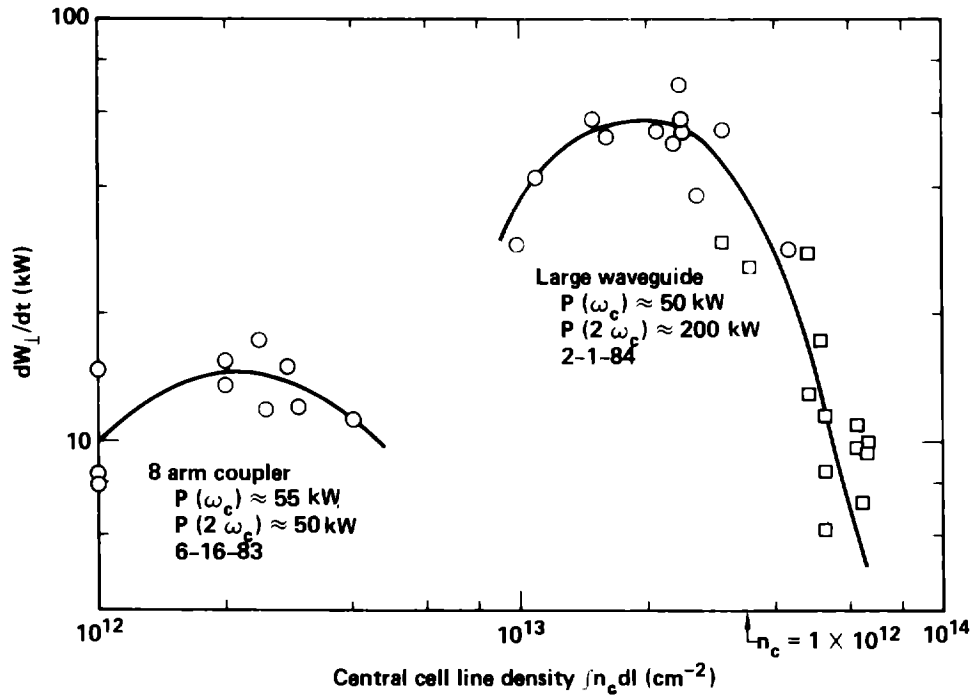


Fig. 11. Variation of hot-electron heating rate in the TMX-U end cell as a function of central-cell density and ECRH power. Plug densities for the 2/1/84 data were in the range  $0.7$  to  $3 \times 10^{12} \text{ cm}^{-3}$ .

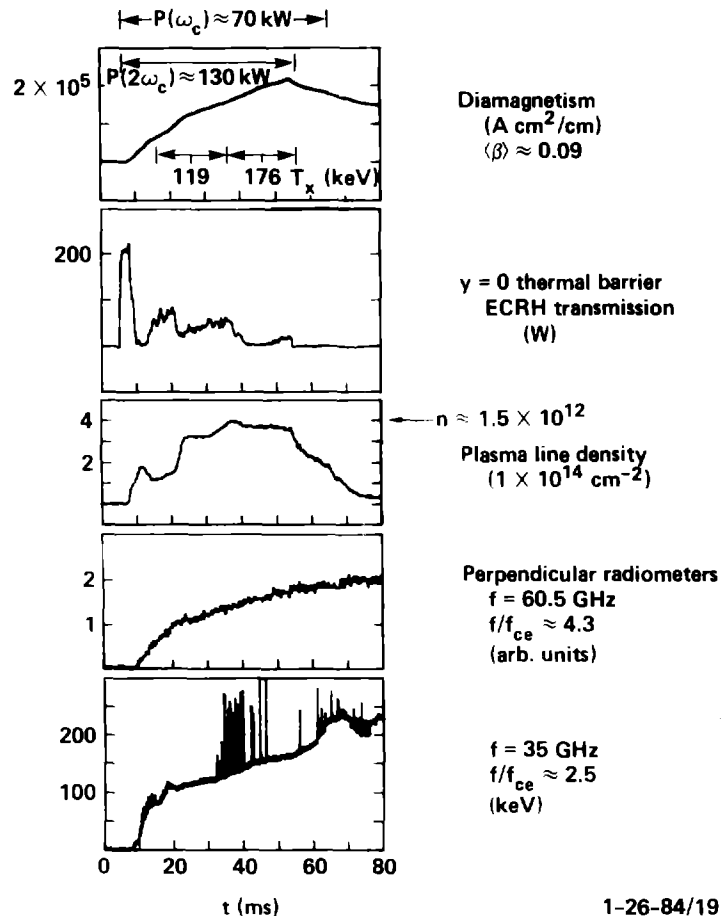


Fig. 12. Typical high-beta hot-electron buildup showing strong ECRH absorption in the thermal barrier and correlation with fluctuations in diamagnetism. Radiometers measure hot-electron emission and non-thermal bursts associated with (weak) instability.

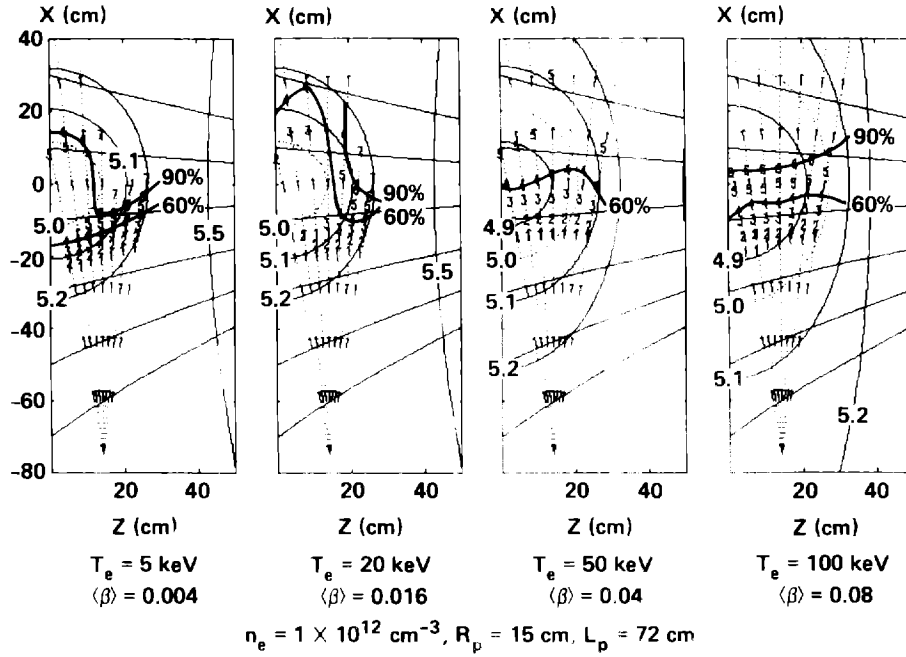


Fig. 13. Ray tracing calculation of absorption in the thermal barrier of TMX-U with constant density and varying temperature. Constant B contours (kG) are noted, as are absorption contours of 60% and 90%. The numbers along the rays and the corresponding absorption are: 1 = 10%, 2 = 20%, 3 = 40%, 4 = 60%, 5 = 80%, 6 = 90%, and 7 = 99%.

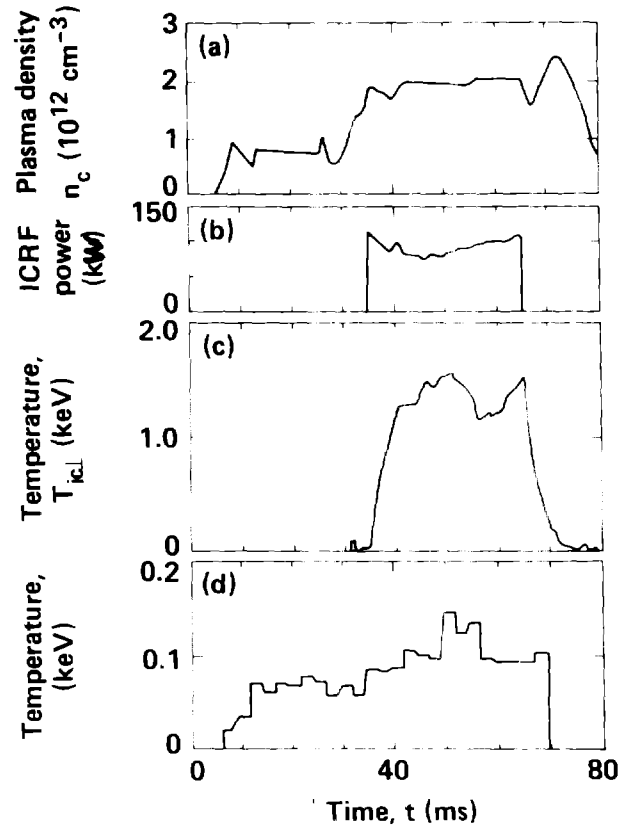


Fig. 14. Heating of ions with ICRH in the TMX-U central cell, showing (a) central density, (b) ICRH antenna power, (c) central-cell ion perpendicular temperature deduced from diamagnetism and density, and (d) parallel temperature of ion end loss.

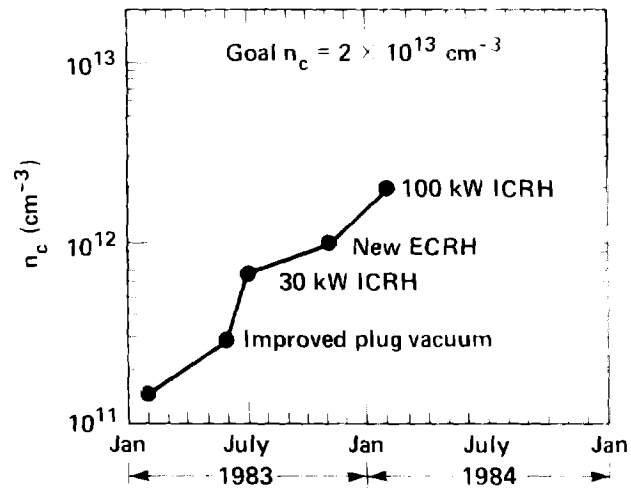


Fig. 15. Increases in central-cell density for plugging, which results from improvements in the plug vacuum and increases in ECRH and ICRH power.